Ceramics International 44 (2018) 8087–8093

Contents lists available at ScienceDirect

Ceramics International

journal homepage: www.elsevier.com/locate/ceramint

Stabilization of α-$BiFeO_3$ structure by Sr^{2+} and its effect on multiferroic properties

F. Pedro-García[a], A.M. Bolarín-Miró[a], F. Sánchez-De Jesús[a,*], C.A. Cortés-Escobedo[b], Z. Valdez-Nava[c], G. Torres-Villaseñor[d]

[a] Área Académica de Ciencias de la Tierra y Materiales, Universidad Autónoma del Estado de Hidalgo Mineral de la Reforma, 42184 Hidalgo, México
[b] Instituto Politécnico Nacional, Centro de Investigación e Innovación Tecnológica, 02250 Ciudad de México, México
[c] LAPLACE, Université de Toulouse, CNRS, INPT, UPS, Toulouse, France
[d] Instituto de Investigaciones en Materiales-UNAM, Ciudad de México, México

ARTICLE INFO

Keywords:
Bismuth ferrite
Strontium doped $BiFeO_3$
Multiferroic
High-energy ball milling
Mechanochemical processing

ABSTRACT

We report a study on the effect of the substitution of Bi^{3+} by Sr^{2+} on the stabilization of *R*3*c* structure of $Bi_{1-x}Sr_xFeO_3$ ($0 \leq x \leq 0.3$, $\Delta x = 0.05$), and its effect in the magnetic and dielectric behavior. Stoichiometric mixtures of Bi_2O_3, Fe_2O_3 and SrO were mixed and milled for 5 h using a ball to powder weight ratio of 10:1 by high-energy ball milling. The obtained powder were pressed at 900 MPa to obtain cylindrical pellets and sintered at 800 °C for 2 h. X-ray diffraction and Rietveld refinement were used to evaluate the effect of Sr^{2+} on the crystal structure. In addition, vibrating sample magnetometry (VSM) and dielectric tests were used for describing the multiferroic behavior. The results show that Sr-doped $BiFeO_3$ particles present rhombohedral structure (*R*3*c*) characteristic of α-$BiFeO_3$ when the doping is below 0.10 mol of Sr. Additionally, a gradual decrease in the amount of secondary phases with the increase of the amount of strontium is observed. For doping concentration higher than 0.15 mol of Sr, a phase transition to an orthorhombic symmetry (β-$BiFeO_3$, *Pbnm*) is detected. Besides, changes in relative intensities of reflection peaks planes (110) and (104) are associated with the phase transformations and with the magnetic and dielectric behavior. The α-$BiFeO_3$ phase show antiferromagnetic behavior and high values of dielectric permittivity, whereas the β-$BiFeO_3$ phase show a ferromagnetic behavior and low dielectric permittivity.

1. Introduction

Bismuth ferrite ($BiFeO_3$) has a perovskite crystal structure distorted in the [111] direction and crystallizes in rhombohedral space group *R*3*c* [1–3]. The lattice parameters are a = 3.965 Å and α = 89.35° [4]. It shows a multiferroic behavior; this term is attributed to materials that show simultaneously two of three ferroic behaviors: ferroelectricity, ferromagnetism, and ferroelasticity. Currently, includes antiferromagnetism, and ferrimagnetism behaviors. $BiFeO_3$ is the only ceramic material that exhibits a multiferroic behavior (ferroelectricity and antiferromagnetism) above the room temperature. It has two transition temperatures, the first is an antiferromagnetic Néel temperature (T_N) at 370 °C, and second the ferroelectric transition with Curie temperature (T_C) at 830 °C [5].

The electronic polarization in $BiFeO_3$ is caused by the free electron pair of Bi^{3+}, the magnetization behavior originates from unpaired electrons in *d* orbitals of Fe^{3+} ions located at B positions [6]. Bismuth ferrite shows an antiferromagnetic behavior, modulated by the Dzyaloshinskii-Moriya interaction. This interaction can be explained in three steps: (i) the antiferromagnetism G-type, that is, each Fe^{3+} with spin-up the nearest Fe^{3+} neighbors have spin-down, (ii) the oxygen octahedra are buckled in order to fit into a small unit cell, it causes a bond distortion on Fe-O-Fe of 156°, generating a weak ferromagnetic moment canceling the AF G-type, and (iii) this weak ferromagnetic moment corresponds with a cycloidal modulation of the spin structure, whose modulation vector has a long period of λ = 64 nm [7,8].

Due to the interest to improve the properties of the $BiFeO_3$, there are many studies focused in modify the magnetic and ferroelectric properties of bismuth ferrite by substituting a cation either in sites A or site B (Bi and Fe, respectively) [3]. Different authors have recently proposed a simple way to change the antiferromagnetic order, by substituting Fe^{3+} by ions of transition metals, like Mn^{3+} or Ti^{4+}. However, these dopants downgrade the ferroelectric behavior, limiting their technological applications [9,10].

The main limitation in the use of the $BiFeO_3$ as material for electronic devices is because it has a high leakage current, this is mainly

* Corresponding author.
E-mail address: fsanchez@uaeh.edu.mx (F. Sánchez-De Jesús).

https://doi.org/10.1016/j.ceramint.2018.01.251
Received 8 November 2017; Received in revised form 11 January 2018; Accepted 29 January 2018
Available online 31 January 2018

because to the formation of secondary phases, as sillenite ($Bi_{25}FeO_{40}$) and mullite ($Bi_2Fe_4O_9$). Different studies have demonstrated that the substitution of A site (Bi^{3+}) by rare-earth ions, like La^{3+} [11], Gd^{3+} [12], Nd^{3+} [13], Sm^{3+} [14], Y^{3+} [15], and Ho^{3+} [16], prevents the precipitation of secondary phases through the stabilization of $BiFeO_3$. However, these dopants decreased the electric polarization of the material. Therefore, is necessary to use a dopant which prevent the formation of secondary phases, without reduce its dielectric properties, which implies to stabilize the rhombohedral crystal structure of $BiFeO_3$ (*R3c*), responsible of the electric polarization.

The Sr^{2+} has been reported to inhibit the appearance of secondary phases like sillenite and mullite, and also, stabilizes the rombohedral crystal structure of $BiFeO_3$; this in turn, decreases the leakage current [17,18]. The addition of dopants, with large ionic radius as Sr^{2+} should generates a slight deformation on the crystal structure, enhancing the magnetic and dielectric properties of $BiFeO_3$.

The synthesis of Sr^{2+} doped $BiFeO_3$ was reported by Bhushan et al. [19]. They used sol-gel synthesis method and doping in the range from 0 to 0.07 mol of Sr^{2+}. They described the relationship between the concentration of Sr and the relative intensities of some diffraction peaks of the XRD patterns, particularly with some called "twin peaks" corresponding to the lattice planes (104) and (110), (006) and (202), (116) and (122) and (018) and (214) and observed than content of strontium increase the relative intensity of lattice plane (104) decreases, they can not identified a phase transition due the low amounts of Sr. Rangi et al. [20] synthesized doped $BiFeO_3$ by solid-state reaction, using as doping agents Ba^{2+}, Sr^{2+}, La^{3+} and Ca^{2+}, doping with 0.20 mol of dopant. They reported an antiferromagnetic or weak ferromagnetic behavior for all the doped compositions. Similar work was done by Wang et al. [21], they synthetized $Bi_xSr_{1-x}FeO_3$ (x = 0.1, 0.2 and 0.3), detecting a possible transition from rhombohedral to triclinic phase, which was associated with the appearing of ferromagnetism. Chu et al. [22] related the inhibition effect in leakage current by doping $BiFeO_3$ with Ca^{2+}, Sr^{2+} and Ba^{2+}, synthesized by solid-state reaction. Dahiya et al. [23] studied the doping with Sr^{2+}in $BiFeO_3$. They showed that strontium enhances the dielectric permittivity. Mao et al. [24], synthesized a co-doped ferrite with Eu^{3+} and Sr^{2+}, and related the increase in Sr content with vanishing of the peak corresponding to the plane (104), due to a structural distortion. Recently, Thakur et al. [25] have carried out an extensive study about the doping effect of Sr in different types of Fe, Mn and Y perovskites, concluding that there is a phase transformation because of the presence of Sr^{2+}.

Although there are several works about the effect of Sr^{2+} on some properties of $BiFeO_3$, there is not yet a clear explanation about the effect of Sr^{2+}on crystal structure changes, and its effect on multiferroic properties of $BiFeO_3$, which is basic information for its prospective application as multiferroic material.

2. Experimental

Fe_2O_3 (Sigma Aldrich, 99% purity), Bi_2O_3 (Sigma Aldrich, 99.9% purity) and SrO (Sigma Aldrich, 99% purity), powders were used as precursor materials. These powders were mixed in a stoichiometric ratio according to the following equation:

$$(1-x)Bi_2O_3 + Fe_2O_3 + 2xSrO + x/2O_2 \rightarrow 2\ \ Bi_{1-x}Sr_xFeO_3 \qquad (1)$$

A mixture, 5 g in total, of precursor materials was loaded along with steel balls of 1.27 cm diameter in a cylindrical steel vial (50 cm^3) (steel/steel, S/S) at room temperature in ambient air and milled for 5 h using a shaker mixer mill (SPEX model 8000D). The ball to powder weight ratio was 10:1. In order to prevent overheating, the milling procedure was carried out in cycles of 90 min of milling and 30 min of standby. The milled powders were uniaxially pressed into pellets using a 10 mm diameter die under 900 MPa pressure on a hydraulic press and sintered at 800 °C for 2 h in air atmosphere. These experimental conditions were selected according to previously described procedures [26–28]. The crystalline phases were characterized by X-ray diffraction (XRD) using a Siemens D5000 diffractometer with CuKα1 radiation (λ = 1.541874 Å). The patterns were recorded in a *2θ* interval of 20–80° with increments of 0.02° (2θ). Rietveld refinements were carried out on the X-ray diffraction patterns using the MAUD software to obtain the percentages of different phases, crystallite sizes, and the microstrain of the materials produced. Rietveld method takes into account all of the information collected in a particular pattern, and it uses a least-squares approach to refine the theoretical line profile until it matches the measured profile [29]. The crystallographic data were obtained from the Inorganic Crystal Structure Database (ICSD).

Magnetic studies were performed at room temperature (25 °C) using a MicroSense EV7 vibrating sample magnetometer with a maximum field of 18 kOe. In order to study their dielectric properties, the sintered pellets were sputtered with gold in both sizes. The dielectric properties were measured using a Broadband Dielectric Spectrometer (Alpha-A, Novocontrol) and controlled the temperature by Quatro Cryosystem in a temperature range from − 140° to 200 °C (ΔT = 20 °C) in the frequency range from 10^{-1} to 10^6 Hz.

3. Results and discussion

Fig. 1 shows the X-ray diffraction (XRD) patterns for different stoichiometric mixtures of Bi_2O_3, Fe_2O_3 and SrO, milled for 5 h, compacted and sintered at 800 °C for 2 h to obtaining different concentration of $Bi_{1-x}Sr_xFeO_3$ ($0 \le x \le 0.3$, $\Delta x = 0.05$). Due to the relevance in the study of low contents of Sr^{2+}, it was studied two extra composition with x = 0.01 and 0.03 mol of Sr^{2+}.

As can be observed in Fig. 1, the X-ray diffraction pattern corresponding to un-doped $BiFeO_3$ (x = 0), shows a mixture of two phases. The perovskite phase, $BiFeO_3$ (ICSD #75324, *R3c*), in a higher proportion (~ 97 wt% according to Rietveld refinement) which is characterized by the presence of “twin peaks”, the most important located around 32° of 2-theta, and a minority phase (~ 3 wt% according to Rietveld refinement), called mullite, $Bi_2Fe_4O_9$ (ICSD #26808, *Pbam*). The presence of mullite is attributed to the synthesis method, which produces unavoidable a small amounts of secondary phases [1].

After doping with low contents of strontium (x = 0.01 and 0.03 mol), the mullite phase still appears, it means that these quantities of strontium are not enough to avoid the precipitation of secondary phases. Conspicuously, increasing a slight the content of strontium up to x = 0.05, the secondary phase completely disappear, and the XRD pattern correspond to pure phase of bismuth ferrite (ICSD #75324, *R3c*).

For higher content of strontium than x = 0.10, it can be observed

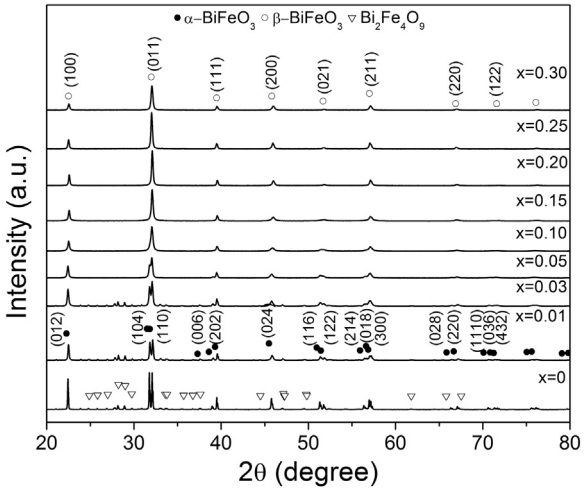

Fig. 1. XRD patterns of compacts of mixtures of Bi_2O_3, Fe_2O_3 and SrO milled for 5 h and sintered at 800 °C for obtaining $Bi_{1-x}Sr_xFeO_3$ varying x, from 0 to 0.30 mol.

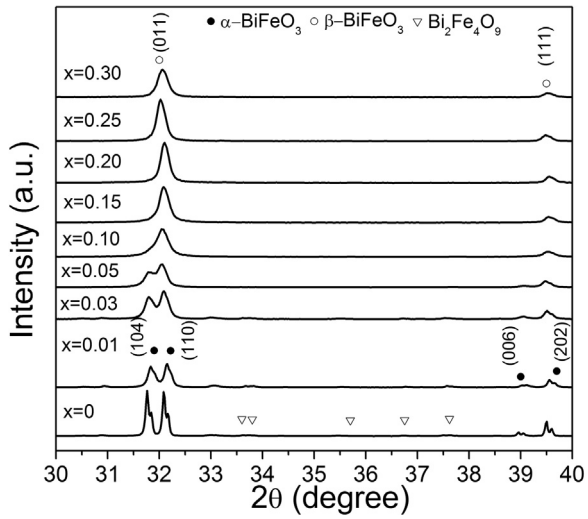

Fig. 2. Interval 2θ, from 30° to 40°, of XRD patterns of compacts of mixtures of Bi_2O_3, Fe_2O_3 and SrO milled for 5 h and sintered at 800 °C for obtaining $Bi_{1-x}Sr_xFeO_3$ varying x, from 0 to 0.30 mol.

that for these materials, peaks corresponding to secondary phase have disappear and some diffraction peaks of the $BiFeO_3$ have vanished, this is attributed to the polymorphic transformation of the $BiFeO_3$, from rhombohedral, *R3c* to orthorhombic, *Pbnm.* This phase is a high-temperature phase of $BiFeO_3$, mentioned by Čebela et al. [30], unexpected at room temperature and stable at temperature above 830 °C.

This effect was reported by Bhushan et al. [19], which studied the substitution of $BiFeO_3$ by different cations substituting A sites (Bi^{3+} positions). They demonstrated that the doping in A sites causes crystal distortion, and it can be quantified through the relative intensity of the "twin peaks". Besides, they found the polymorphic (*R3c* to *Pbnm*) transformation for high contents of dopant.

The phase transition from a phase rhombohedral (α-$BiFeO_3$), *R3c*, to one of greater symmetry orthorhombic (β-$BiFeO_3$), *Pbnm,* and with many systematic cancellations, is easily observable as a decrement of the intensity of one of the "twin peaks" in the XRD patterns, and the elimination of secondary phases.

Fig. 2 shows an amplified of the XRD pattern from 30° to 40° and the XRD pattern of un-doped $BiFeO_3$ (x = 0) confirms the presence of two peaks or "twin peaks" in ~ 31.7° and ~ 32.2° corresponding to (1 0 4) and (1 1 0) crystallographic planes, respectively; Besides, it can be observed a small peaks (alongside each peak), they correspond to the diffraction of Kα2, which match with the report in de ICSD target of $BiFeO_3$ (ICSD #75324, *R3c*). Increasing the amount of Sr until 0.10, a slight intensity diminution of the peak located at 31.7° can be observed, this peak correspond to crystallographic plane (1 0 4). While, the peak corresponding to the crystallographic plane (1 1 0) keeps its position in 2θ and increases its intensity. For higher level of strontium than 0.15 mol, the peak (104) has completely disappeared, and there is only the peak (110). This phenomenon also occurs in "twin peaks" along the XRD pattern, therefore, all the "twin peaks" transform to single peaks with the amount of Sr increments.

It is especially important the analysis of "twin peaks" located at around 39° of 2θ, corresponding to the diffraction of the planes (006) and (202), it lets to identify the polymorphic phase transition. In good agreement with Kumar et al. [31], the results allow us to conclude that plane (006) is characteristic of the rhombohedral structure, and this plane influences the ternary axis of the symmetry *R3c*, which is distorted by means of doping with Sr. The presence of this peak diffraction in XRD pattern displays, to a great extent, if the structural transition from rhombohedric to orthorhombic has already occurred.

Rietveld refinements were carried out to study the evolution of the cell parameters, crystallite size and microstrain with the strontium content (Table 1). As it can be observed, the presence of $Bi_2Fe_4O_9$ (mullite) as secondary phase decreases with the strontium content, and above 0.10 mol of strontium, this phase is not detected. Additionally, this amount of Sr^{2+} substitution (0.10 mol.) could be the solubility limit of Sr^{2+} in α-$BiFeO_3$. Increasing the Sr^{2+} content promotes an increase in the microstrain induced by Sr^{2+} substitution into the crystal structure, which promotes the structural transformation from rhombohedral to orthorhombic. In addition, these results confirm that nanocrystalline $BiFeO_3$ with a crystallite size of approximately 140 nm was obtained by high-energy ball milling assisted with annealing. The refinement parameters show a good adjustment, as it can be observed in Table 1, with the value of χ^2 less than 2.

Figs. 3–5 show the magnetic hysteresis loops of the different stoichiometric mixtures of Bi_2O_3, Fe_2O_3 and SrO milled for 5 h and annealed at 650 °C for obtaining $Bi_{1-x}Sr_xFeO_3$ varying x, from 0 to 0.30 mol.

In Fig. 3, where the hysteresis loops for doped level from x = 0 (undoped) to 0.03 are presented, it can be observed that all the compositions show similar antiferromagnetic (AF) order, related to rhombohedral α-$BiFeO_3$ and in good agreement with the XRD results. The secondary phase, $Bi_2Fe_4O_9$, does not influence the magnetic behavior because it exhibits antiferromagnetic nature [32]. Besides, it is not possible to detect the effect of strontium as all the compositions show the same magnetic behavior, the hysteresis loops are overlapping, showing a specific magnetization of ~ 0.13 emu/g at 18 kOe, in good agreement with previous reports [1].

As it is presented in Fig. 4, when the concentration of ion strontium is increased up to 0.15 mol, the magnetic behavior change to weak ferromagnetism, with low specific magnetization (~ 0.12 emu/g at 18 kOe) and low magnetic remanence (~ 0.002 emu/g). According to the XRD pattern and Rietveld refinement shown in Fig. 1 and Table 1, for this doped levels, the material is near to pure α-$BiFeO_3$ (rhombohedral, *R3c*), and there are not secondary phases. Therefore, the weak ferromagnetism must be attribute to the presence of strontium

Table 1
Rietveld analysis of the XRD pattern of pellets of all compositions.

Sr doped level, x (mol)	$BiFeO_3$				$Bi_2Fe_4O_9$			χ^2
	Crystallite size (nm)	Phase (wt%)	Microstrain (*10–5)	Space group	Crystallite size(nm)	Phase (wt%)	Space group	
0	142.57 ± 2.40	93.46 ± 1.91	40.31 ± 3.24	*R3c*	127.34 ± 1.23	6.54 ± 1.07	*I23*	1.31
0.01	145.31 ± 2.50	95.35 ± 1.92	41.17 ± 2.37	*R3c*	132.45 ± 2.11	4.65 ± 1.16	*I23*	1.27
0.03	127.21 ± 1.81	94.93 ± 1.32	41.09 ± 4.87	*R3c*	145.13 ± 3.01	3.09 ± 1.18	*I23*	1.11
0.05	137.87 ± 2.10	96.84 ± 1.97	56.21 ± 7.31	*R3c*	*	*	–	1.39
0.10	140.34 ± 1.92	96.54 ± 1.93	67.34 ± 3.57	*R3c*	*	*	–	1.51
0.15	142.65 ± 1.91	100 ± 1.51	69.79 ± 6.71	*Pbnm*	*	*	–	1.29
0.20	139.49 ± 2.17	100 ± 2.04	73.92 ± 5.49	*Pbnm*	*	*	–	1.74
0.25	128.46 ± 2.01	100 ± 3.49	75.35 ± 3.81	*Pbnm*	*	*	–	1.52
0.30	130.98 ± 1.90	100 ± 2.98	80.13 ± 4.41	*Pbnm*	*	*	–	1.25

* Not detectable.

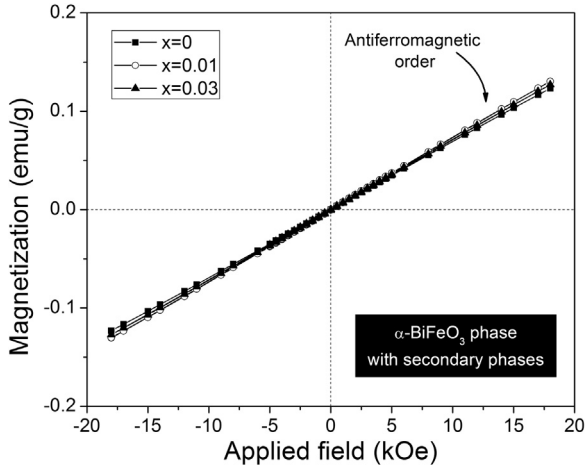

Fig. 3. Hysteresis magnetic loops of mixtures of Bi_2O_3, Fe_2O_3 and SrO sintered at 800 °C for 2 h for obtaining $Bi_{1-x}Sr_xFeO_3$ varying x, from 0.0 to 0.03 mol.

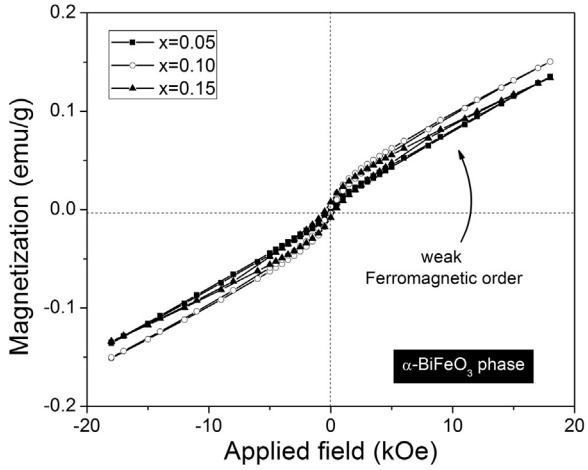

Fig. 4. Hysteresis magnetic loops of mixtures of Bi_2O_3, Fe_2O_3 and SrO sintered at 800 °C for 2 h for obtaining $Bi_{1-x}Sr_xFeO_3$ varying x, from 0.05 to 0.15 mol.

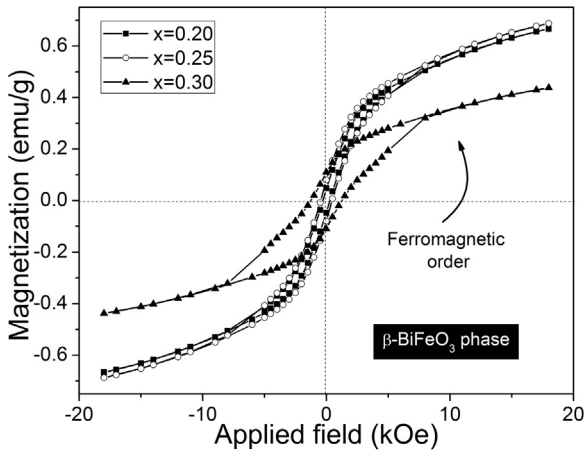

Fig. 5. Hysteresis magnetic loops of mixtures of Bi_2O_3, Fe_2O_3 and SrO sintered at 800 °C for 2 h for obtaining $Bi_{1-x}Sr_xFeO_3$ varying x, from 0.20 to 0.30 mol.

concentration into the crystal structure. At this point, the magnetic contribution of the strontium begins to be noticeable, and it is able to distort the crystal structure, modifying the spin cycloid structure and promoting the weak ferromagnetism in this material.

The magnetic hysteresis loops corresponding to 0.20, 0.25 and 0.30 mol. of strontium are presented in Fig. 5, where a ferromagnetic order is observed with specific magnetization between 0.43 and 0.66 emu/g at 18 kOe, for x equal to 0.30 and 0.25, respectively. Besides, the remanent magnetization has been increased in reference with lower contents of strontium, achieving values of 0.11 emu/g. These values are associated to the formation of β-$BiFeO_3$ (orthorhombic, *Pbnm*), which is characterized by a ferromagnetic order [33]. Additionally, for these compositions, the increase in coercivity is considerably, especially for high doping concentration (x = 0.30); it shows a high coercivity, about 1.5 kOe. This effect can be attributed to the substitution of Bi^{3+} by Sr^{2+} into the crystal structure, due to ionic radii of strontium is larger than the ionic radii of bismuth, 1.18 Å and 1.03 Å, respectively [34], promoting the internal stresses, the deformation and as a consequence, an increase in the coercivity of the material.

Table 2
Specific magnetization (Ms at 18 kOe), coercive field (Hc), remanent magnetization (Mr), mass magnetic susceptibility (χ_m) and space group (from XRD) for $Bi_{1-x}Sr_xFeO_3$ varying x, from 0 to 0.30 mol.

Sr level content x (mol)	Magnetic order	M_s at 18 kOe (emu/g)	H_c (kOe)	M_r (emu/g)	χ_m (10^{-8} m^3/kg)	Space group
0	Antiferromagnetic	0.120	–	–	0.683	*R3c*
0.01	Antiferromagnetic	0.130	–	–	0.722	*R3c*
0.03	Antiferromagnetic	0.127	–	–	0.706	*R3c*
0.05	Weak ferromagnetic	0.135	–	0.002	–	*R3c*
0.10	Weak ferromagnetic	0.151	–	0.004	–	*R3c*
0.15	Weak ferromagnetic	0.134	–	0.008	–	*Pbnm*
0.20	Ferromagnetic	0.666	0.25	0.040	–	*Pbnm*
0.25	Ferromagnetic	0.687	0.50	0.080	–	*Pbnm*
0.30	Ferromagnetic	0.437	1.50	0.110	–	*Pbnm*

In Table 2, are tabulated the magnetic parameters as a function of the strontium concentration, materials with rhombohedral phase show an antiferromagnetic order behavior. The results support the idea that the antiferromagnetic order is frustrated by the substitution of Bi^{3+} by Sr^{2+} for low strontium contents. When the amount of strontium is higher than 0.15 mol. occurs the phase transition from *R3c* to *Pbnm*, which can be detected as a change from weak ferromagnetic to ferromagnetic behavior, with high coercivity.

The effect of strontium concentration in $BiFeO_3$ on the relative permittivity versus frequency at room temperature is shown in Fig. 6. It can be explained based on space charge polarization due to inhomogeneites present in the dielectric structure like secondary phases or porosity (ascribed to the conformation process). For low strontium contents, (< 0.10), the sintered pellets present similar behavior. They show high permittivity in a range of low frequencies. This phenomenon agrees with the Maxwell-Wagner model that indicates that in low

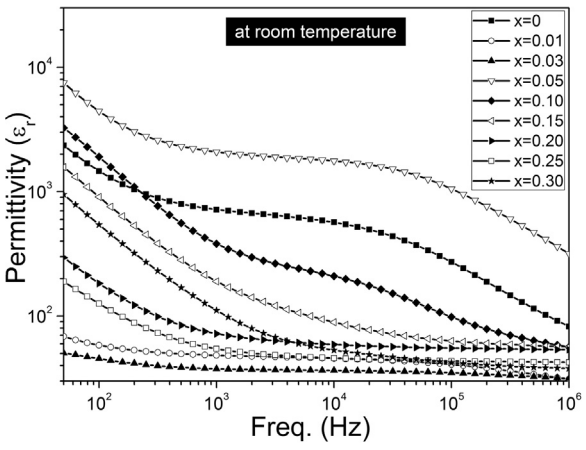

Fig. 6. Relative permittivity versus frequency of $Bi_{1-x}Sr_xFeO_3$ varying x, from 0 to 0.30 mol.

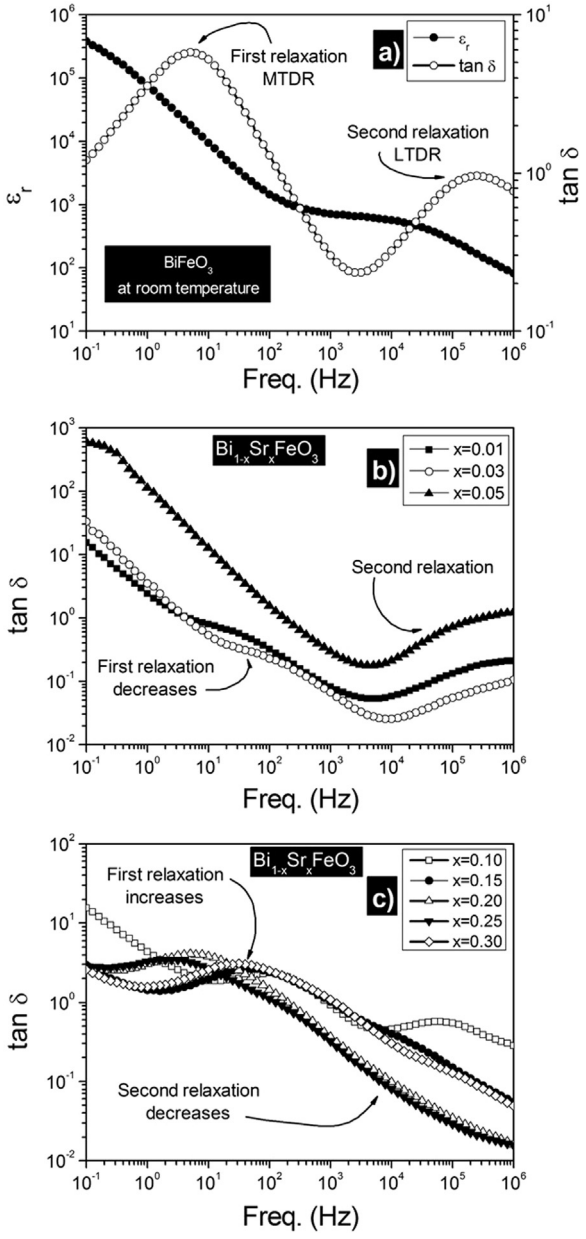

Fig. 7. (a) Dependent frequency of dielectric permittivity and tan δ of BiFeO3, (b) Dependent frequency of tan δ of (b) x = 0.01–0.05 and (c) x = 0.10–0.30 of Bi1-xSrxFeO3 system.

frequencies (< 100 kHz) the main contributors to the dielectric constant are the charge displacement, and these are usually within the limits of the dielectric layer (grain boundaries, vacancies, defects) [35]. When the frequency is higher than the Maxwell-Wagner model indicates, the polarizable charges are not able to follow the applied field and the induced dipoles do not have time to relax, this is depicted as a decrease in the dielectric constant in the range of high frequencies [36,37]. For higher strontium content, from 0.15 to 0.30 mol, it can observe a decrease in values of dielectric permittivity is observed in the whole range of measured frequencies. This behavior indicates a lower dielectric response, typically presented for β-$BiFeO_3$ structure [33]. This agrees with the phase transition from *R3c* to *Pbnm*, described previously by means of XRD for x higher than 0.10. For these compositions, the material shows pure orthorhombic phase.

The dielectric permittivity and tan δ vs frequency plots are shown in Fig. 7a. The corresponding to x = 0 ($BiFeO_3$) shows two dielectric relaxations indicated for the maximum values of tan δ, the first corresponds to Middle Temperature Dielectric Relaxation (MTDR) and the second to Low Temperature Dielectric Relaxation (LTDR), following the Hunpratub nomenclature [38]. As can be observed in the Fig. 7b MTDR decrees with the increment of Sr in the crystal structure, specifically in x = 0.01 and 0.03, MTDR might be related to the microstructure, in particular, to the grain boundary, grain sizes, defect structure and closely with $Bi_2Fe_4O_9$ as secondary phase acting as an additional internal barrier layer making the heterogeneity more complex [39]. Otherwise, the sample without secondary phases (x = 0.05) just has a MTDR. When the amount of strontium is increased to 0.10, an anomaly is seen, it presents again two relaxations but they are no clearly identifiable due the overlapping of all samples. In x = 0.15–0.30 compositions, shown in Fig. 7c, the MTDR there are no logger present, only the relaxation corresponding to LTDR appears. This can be related to the mixed valence of the Fe^{2+}, Fe^{3+} and the substitution of Bi^{3+} to Sr^{2+} ions, the phenomena is explained by the charge transfer between 2+ and 3+ ions leads to the hopping conduction of the localized charge carrier inside the grain [40]. Although there is not a report indicating the dielectric behavior when there is a phase transition, a clear correlation can be seen between α-$BiFeO_3$ with secondary phases, pure α-$BiFeO_3$ and β-$BiFeO_3$. In order to have more proof of this, were calculated the activation energies of the observed MTDR and LTDR relaxations with data obtained at different temperatures (Fig. 8). After fitting the data to an Arrhenius linearization, it can seen in the Table 3 that for each relaxation temperature, the activation energies have similar values for LTDR (− 140 to 20 °C) and MTDR (20–200°) in all the samples, it confirms the relation of these dielectric relaxations to the crystallography of the studied compositions.

The relationship between crystalline structure, magnetic and dielectric properties can be described as follows. When strontium is introduced into the α-$BiFeO_3$ crystal structure a distortion is induced to FeO_6 octahedron and Fe–O–Fe bond angle tends to 180°, iron returns to its centrosymmetric position and the plane (110) increase the planar density. Therefore, the plane (104) undergoes to decrease in its planar density due to Sr^{2+} has larger ionic radii than Bi^{3+} [34], then it takes a centrosymmetric position. This, in turn, reduces the spontaneous dielectric polarization and increases the specific magnetization, in good agreement with the experimental results, presented above. In order to facilitate the comprehension, a schematic representation of the α-$BiFeO_3$ structure is shown in Fig. 9a, where it is observed that two cubes represent one-unit formula, these cubes share a corner and form rhombohedra between the two unit cell of $BiFeO_3$. In Fig. 9b, the unit cell of the $BiFeO_3$ is presented, the axis $[0\ 0\ 1]_{Hex}$ is analogous to $[111]_{Rh}$, in this gives spontaneous polarization because Bi and Fe are offset from their centrosymmetric position by the distortion in the Fe–O–Fe bond at 154–156°. This bond distortion is caused by the

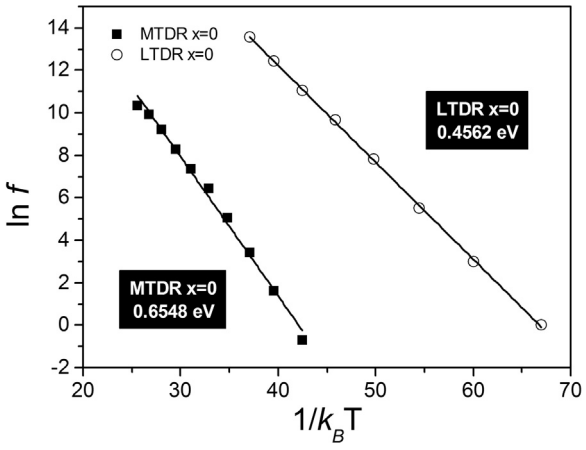

Fig. 8. Activation energies for LTDR and MTDR processes plotted as a function of reciprocal temperature of $BiFeO_3$.

Table 3
Frequency of first and second relaxation in tanδ Vs Freq plots, activation energies and space (from XRD) for $Bi_{1-x}Sr_xFeO_3$ varying x, from 0 to 0.30 mol.

Sr level content, x	tanδ		U		Space group
	2nd Relaxation (Hz)	1st Relaxation (Hz)	MTDR (eV)	LTDR (eV)	
0	5.00E+00	2.51E+05	0.6548 ± 0.017	0.4562 ± 0.003	*R3c*
0.01	6.30E+01	1.00E+06	0.6135 ± 0.012	0.4030 ± 0.004	*R3c*
0.03	1.00E+02	1.00E+06	0.5947 ± 0.014	0.4025 ± 0.004	*R3c*
0.05	–	7.94E+05	–	0.4035 ± 0.005	*R3c*
0.1	1.25E+02	6.31E+04	0.5520 ± 0.012	0.4789 ± 0.003	*R3c*
0.15	5.01E+01	–	0.5933 ± 0.007	–	*Pbnm*
0.2	6.30E+00	–	0.6532 ± 0.011	–	*Pbnm*
0.25	3.49E+00	–	0.5363 ± 0.055	–	*Pbnm*
0.3	3.05E+00	–	0.6045 ± 0.006	–	*Pbnm*

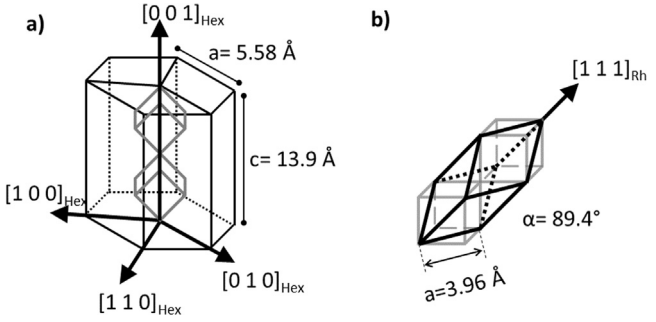

Fig. 9. Schematic representation of (a) hexagonal and (b) rhombohedral structure of the bismuth ferrite.

octahedron FeO_6 buckle in order to fit into a small unit cell. If amount of Sr is increased the cell angles increased from 89.4° to 90°, adopting a β-$BiFeO_3$ with orthorhombic structure, as consequence, decreasing the spontaneous polarization and increasing the specific magnetization, due α-β phase transition.

4. Conclusions

Strontium-doped bismuth ferrite ($Sr_xBi_{1-x}FeO_3$, $0 \leq x \leq 0.3$) powders with crystallite sizes of approximately 140 nm have been successfully produced by high-energy ball milling for 5 h, and annealing at 800 °C for 2 h. X-ray diffraction technique confirmed the obtaining of α-$BiFeO_3$ with rhombohedral structure for $x < 0.10$. At low strontium contents ($x \leq 0.03$), small amounts of secondary phase (mullite, $Bi_2Fe_4O_9$) are identified. At strontium doping $x = 0.05$, the secondary phase cannot be detected by XRD. Strontium doping concentrations higher than $x > 0.1$ produce a phase transformation from α-$BiFeO_3$ (rhombohedral, *R3c*) to β-$BiFeO_3$ (orthorhombic, *Pbnm*). In addition, the changes in the main diffraction peaks corresponding to the planes (110) and (104) were associated to the magnetic and dielectric behavior of the samples. When the relative intensity of the plane (110) decreases, due to the change in planar density by the substitution of Bi to Sr, a better dielectric behavior ($\varepsilon_r \approx 3000$) is obtained, and tends to decrease the specific magnetization of antiferromagnetic behavior from 0.13 to 0.015 emu/g. These effects were attributed to the absence of secondary phases. When $x < 0.15$, the main peaks change to form a single peak, corresponding to the diffraction of the plane (100) of the orthorhombic β-$BiFeO_3$. This phase presents values from 0.13 to 0.6871 emu/g at range doping level from 0.15 to 0.30 M, and for all the samples identified with this phase; a poor dielectric behavior was obtained. Two dielectric relaxation processes in the low and middle temperature range were found to contribute to the dielectric response. The LTDR are in low-doped (0–0.10) samples with Sr characterized by α-$BiFeO_3$ structure, and have activation energies around 0.4 eV. The MTDR is presented in high-doped samples (0.15–0.30) characterized by β-$BiFeO_3$ structure, and have activation energies around 0.6 eV.

References

[1] F. Pedro-García, F. Sánchez-De Jesús, C.A. Cortés-Escobedo, A. Barba- Pingarrón, A.M. Bolarín-Miró, Mechanically assisted synthesis of multiferroic $BiFeO_3$: effect of synthesis parameters, J. Alloy. Compd. 711 (2017) 77e84, http://dx.doi.org/10.1016/j.jallcom.2017.03.292.

[2] F. Kubel, H. Schmid, Structure of a ferroelectric and ferroelastic monodomain crystal of the perovskite $BiFeO_3$, Acta Crystallogr. Sect. B 46 (1990) 698–702, http://dx.doi.org/10.1107/S0108768190006887.

[3] M.M. Kumar, V.R. Palkar, K. Srinivas, S.V. Suryanarayana, Ferroelectricity in a pure $BiFeO_3$ ceramic, Appl. Phys. Lett. 76 (2000) 2764–2766, http://dx.doi.org/10.1063/1.126468.

[4] R. Safi, H. Shokrollahi, Physics, chemistry and synthesis methods of nanostructured bismuth ferrite ($BiFeO_3$) as a ferroelectro-magnetic material, Prog. Solid State Chem. 40 (2012) 6–15, http://dx.doi.org/10.1016/j.progsolidstchem.2012.03.001.

[5] S. Dong, J.-M. Liu, S.-W. Cheong, Z. Ren, Multiferroic materials and magnetoelectric physics: symmetry, entanglement, excitation, and topology, Adv. Phys. 64 (2015) 519–626, http://dx.doi.org/10.1080/00018732.2015.1114338.

[6] J.T. Heron, D.G. Schlom, R. Ramesh, Electric field control of magnetism using $BiFeO_3$-based heterostructures, Appl. Phys. Rev. 1 (2014), http://dx.doi.org/10.1063/1.4870957.

[7] D. Khomskii, Classifying multiferroics: mechanisms and effects, Phys. (Coll. Park. Md) 2 (2009) 20, http://dx.doi.org/10.1103/Physics.2.20.

[8] I. Dzyaloshinskii, On the magneto-electrical effect in antiferromagnets, Sov. Phys. JETP 10 (1960) 628–629, http://dx.doi.org/10.1016/0041-624x(70)90745-6.

[9] N. Yan, Y.L. Zhang, W.L. Tang, S.H. Yang, D.H. Chen, The effects of Mn doping on the optical properties of chemically deposited $BiFeO_3$ thin films, Thin Solid Films 1 (2014) 10–13, http://dx.doi.org/10.1016/j.tsf.2014.03.012.

[10] M.S. Bernardo, T. Jardiel, M. Peiteado, A.C. Caballero, M. Villegas, Sintering and microstructural characterization of W^{6+}, Nb^{5+} and Ti^{4+} iron-substituted $BiFeO_3$, J. Alloy. Compd. 509 (2011) 7290–7296, http://dx.doi.org/10.1016/j.jallcom.2011.04.087.

[11] P. Suresh, S. Srinath, Observation of high coercivity in multiferroic lanthanum doped $BiFeO_3$, J. Alloy. Compd. 554 (2013) 271–276, http://dx.doi.org/10.1016/j.jallcom.2012.11.129.

[12] S.V. Vijayasundaram, G. Suresh, R.A. Mondal, R. Kanagadurai, Composition-driven enhanced magnetic properties and magnetoelectric coupling in Gd substituted $BiFeO_3$ nanoparticles, J. Magn. Magn. Mater. 418 (2015) 30–36, http://dx.doi.org/10.1016/j.jmmm.2016.02.048.

[13] D. Wang, M. Wang, F. Liu, Y. Cui, Q. Zhao, H. Sun, H. Jin, M. Cao, Sol-gel synthesis of Nd-doped $BiFeO_3$ Multiferroic and its characterization, Ceram. Int. 41 (2015) 8768–8772, http://dx.doi.org/10.1016/j.ceramint.2015.03.100.

[14] C.S. Tu, C.S. Chen, P.Y. Chen, H.H. Wei, V.H. Schmidt, C.Y. Lin, J. Anthoniappen, J.M. Lee, Enhanced photovoltaic effects in A-site samarium doped $BiFeO_3$ ceramics: the roles of domain structure and electronic state, J. Eur. Ceram. Soc. 36 (2016) 1149–1157, http://dx.doi.org/10.1016/j.jeurceramsoc.2015.12.019.

[15] N.I. Ilic, J.D. Bobic, B.S. Stojadinovic, A.S. Dzunuzovic, M.M. Vijatovic Petrovic, Z.D. Dohcevic-Mitrovic, B.D. Stojanovic, Improving of the electrical and magnetic properties of $BiFeO_3$ by doping with yttrium, Mater. Res. Bull. 77 (2016) 60–69, http://dx.doi.org/10.1016/j.materresbull.2016.01.018.

[16] N. Van Minh, N. Gia Quan, Structural, optical and electromagnetic properties of $Bi_{1-x}Ho_xFeO_3$ multiferroic materials, J. Alloy. Compd. 509 (2011) 2663–2666, http://dx.doi.org/10.1016/j.jallcom.2010.12.033.

[17] M.R. Islam, R.H. Galib, A. Sharif, M. Hasan, M.A. Zubair, M.F. Islam, Correlation of charge defects and morphology with magnetic and electrical properties of Sr and Ta codoped $BiFeO_3$, J. Alloy. Compd. 688 (2016) 1186–1194, http://dx.doi.org/10.1016/j.jallcom.2016.07.134.

[18] N. Sharma, S. Kumar, A.K. Mall, R. Gupta, A. Garg, Sr and Mn Co-doped sol-gel derived $BiFeO_3$ ceramics with enhanced magnetism and reduced leakage current, Mater. Res. Express 4 (2017) 0–9, http://dx.doi.org/10.1088/2053-1591/aa5579.

[19] B. Bhushan, A. Basumallick, N.Y. Vasanthacharya, S. Kumar, D. Das, Sr induced modification of structural, optical and magnetic properties in $Bi_{1-x}Sr_xFeO_3$ (x = 0, 0.01, 0.03, 0.05 and 0.07) multiferroic nanoparticles, Solid State Sci. 12 (2010) 1063–1069, http://dx.doi.org/10.1016/j.solidstatesciences.2010.04.026.

[20] M. Rangi, A. Agarwal, S. Sanghi, R. Singh, S.S. Meena, A. Das, Crystal structure and magnetic properties of $Bi_{0.8}A_{0.2}FeO_3$ (A = La, Ca, Sr, Ba) multiferroics using

neutron diffraction and Mossbauer spectroscopy, AIP Adv. 4 (2014) 87121, http://dx.doi.org/10.1063/1.4893241.
[21] L.Y. Wang, D.H. Wang, H.B. Huang, Z.D. Han, Q.Q. Cao, B.X. Gu, Y.W. Du, The magnetic properties of polycrystalline $Bi_{1-x}Sr_xFeO_3$ ceramics, J. Alloy. Compd. 469 (2009) 1–3, http://dx.doi.org/10.1016/j.jallcom.2008.01.095.
[22] S. Chu, M. Zhang, H. Deng, Z. Wang, Y. Wang, Y. Pan, H. Yan, Investigation of doping effect on electrical leakage behavior of $BiFeO_3$ ceramics, J. Alloy. Compd. 689 (2016) 475–480, http://dx.doi.org/10.1016/j.jallcom.2016.07.270.
[23] R. Dahiya, A. Agarwal, S. Sanghi, A. Hooda, P. Godara, Structural, magnetic and dielectric properties of Sr and V doped $BiFeO_3$ multiferroics, J. Magn. Magn. Mater. 385 (2015) 175–181.
[24] W. Mao, W. Chen, X. Wang, Y. Zhu, Y. Ma, H. Xue, L. Chu, J. Yang, X. Li, W. Huang, Influence of Eu and Sr co-substitution on multiferroic properties of $BiFeO_3$, Ceram. Int. 42 (2016) 12838–12842, http://dx.doi.org/10.1016/j.ceramint.2016.05.048.
[25] S. Thakur, K. Singh, O.P. Pandey, Sr doped $BiMO_3$ (M = Mn, Fe, Y) perovskites: structure correlated thermal and electrical properties, Mater. Chem. Phys. 187 (2017) 96–103, http://dx.doi.org/10.1016/j.matchemphys.2016.11.052.
[26] A.M. Bolarín-Miró, F. Sánchez-De Jesús, C.A. Cortés-Escobedo, R. Valenzuela, S. Ammar, Structure and magnetic properties of $Gd_xY_{1-x}FeO_3$ obtained by mechanosynthesis, J. Alloy. Compd. 586 (2014) 90–94, http://dx.doi.org/10.1016/j.jallcom.2013.04.029.
[27] A.M. Bolarín-Miró, F. Sánchez-De Jesús, C.A. Cortés-Escobedo, S. Díaz-De la Torre, R. Valenzuela, Synthesis of M-type $SrFe_{12}O_{19}$ by mechanosynthesis assisted by Spark Plasma Sintering, J. Alloy. Compd. 643 (2014) 226–230, http://dx.doi.org/10.1016/j.jallcom.2014.11.124.
[28] F. Sánchez-De Jesús, C.A. Cortés-Escobedo, A.M. Bolarín-Miró, I.A. Lira-Hernández, G. Torres-Villaseñor, Crystal structure and mixed ionic-electronic conductivity of mechanosynthesized $La_{1-x}Ca_xMnO_3$ ($0 < x < 0.8$), Ceram. Int. 38-3 (2012) 2139–2144, http://dx.doi.org/10.1016/j.ceramint.2011.10.055.
[29] L. Lutterotti, S. Matthies, H.-R. Wenk, A.S. Schultz, J.W. Richardson, Combined texture and structure analysis of deformed limestone from time-of-flight neutron diffraction spectra, J. Appl. Phys. 81 (1997) 594, http://dx.doi.org/10.1063/1.364220.
[30] M. Čebela, D. Zagorac, K. Batalović, J. Radaković, B. Stojadinović, V. Spasojević, R. Hercigonja, $BiFeO_3$ perovskites: a multidisciplinary approach to multiferroics, Ceram. Int. 43 (2017) 1256–1264, http://dx.doi.org/10.1016/j.ceramint.2016.10.074.
[31] P. Kumar, M. Kar, Effect of structural transition on magnetic and dielectric properties of la and Mn co-substituted $BiFeO_3$ ceramics, Mater. Chem. Phys. 148 (2014) 968–977, http://dx.doi.org/10.1016/j.matchemphys.2014.09.007.
[32] P.K.S. Rao, S. Krishnan, M. Pattabi, G. Sanjeev, Magnetic and photoluminescence studies of electron irradiated $Bi_2Fe_4O_9$ nanoparticles, J. Magn. Magn. Mater. 401 (2016) 77–80, http://dx.doi.org/10.1016/j.jmmm.2015.10.016.
[33] P. Kumar, C. Panda, M. Kar, Effect of rhombohedral to orthorhombic transition on magnetic and dielectric properties of La and Ti co-substituted $BiFeO_3$, Smart Mater. Struct. 24 (2015) 45028, http://dx.doi.org/10.1088/0964-1726/24/4/045028.
[34] R.D. Shannon, Revised effective ionic radii and systematic studies of interatomic distances in halides and chalcogenides, Acta Crystallogr. Sect. A 32 (1976) 751–767, http://dx.doi.org/10.1107/S0567739476001551.
[35] A.Y. Kim, S.H. Han, H.-W. Kang, H.-G. Lee, J.S. Kim, C.I. Cheon, Dielectric and magnetic properties of $BiFe_O3$ ceramics prepared by hydrothermal synthesis, Ceram. Int. 38 (2011) S397–S401, http://dx.doi.org/10.1016/j.ceramint.2011.05.019.
[36] H. Liu, Y. Pu, X. Shi, Q. Yuan, Dielectric and ferroelectric properties of $BiFeO_3$ ceramics sintered in different atmospheres, Ceram. Int. 39 (2013) S217–S220, http://dx.doi.org/10.1016/j.ceramint.2012.10.065.
[37] P. Godara, A. Agarwal, N. Ahlawat, S. Sanghi, R. Dahiya, Crystal structure transformation, dielectric and magnetic properties of Ba and Co modified $BiFeO_3$ multiferroic, J. Alloy. Compd. 594 (2014) 175–181, http://dx.doi.org/10.1016/j.jallcom.2014.01.103.
[38] S. Hunpratub, P. Thongbai, T. Yamwong, R. Yimnirun, S. Maensiri, Dielectric relaxations and dielectric response in multiferroic $BiFeO_3$ ceramics, Appl. Phys. Lett. 94 (2009), http://dx.doi.org/10.1063/1.3078825 (062904-1-3).
[39] J.C. Chen, J.M. Wu, Dielectric properties and ac conductivities of dense single-phased $BiFeO_3$ ceramics, Appl. Phys. Lett. 91 (2007), http://dx.doi.org/10.1063/1.2798256.
[40] N. Ikeda, H. Ohsumi, K. Ohwada, K. Ishii, T. Inami, K. Kakurai, Y. Murakami, K. Yoshii, S. Mori, Y. Horibe, H. Kitô, Ferroelectricity from iron valence ordering in the charge-frustrated system $LuFe_2O_4$, Nature 436 (2005) 1136–1138, http://dx.doi.org/10.1038/nature04039.